

Numerical modeling of copper-steel laser joining

I.Tomashchuk*, J.-M. Jouvard, P. Sallamand

Institut Carnot de Bourgogne, Université de Bourgogne, ICB-IRM-LTm, 12 rue de la Fonderie, F-71200 Le Creusot, France

*Institut Carnot de Bourgogne, Université de Bourgogne, ICB-IRM-LTm, 12 rue de la Fonderie, F-71200 Le Creusot, France, iryana.tomashchuk@u-bourgogne.fr

Abstract: Our research is dedicated to the joining of stainless steel AISI 316 L with copper by high-powered laser Nd:YAG welding. In course of our work we develop the numerical model of laser welding process which relies on correspondence with experimental data.

Keywords: dissimilar laser welding, heat transfer, convection, diffusion, element analysis.

1. Introduction

Dissimilar joining of metals is the subject of numerous investigations due to its high technical and economical potential. But using of conventional techniques of welding often poses metallurgical problems (cracking, deformation, short life of the weld etc.) resulting from very different fusion temperature, thermal expansion, thermal conductivity and other parameters. High powered laser welding (10^{10} W/cm²) permits to solve these problems by creating very high and local thermal gradient (1).

Dissimilar laser welding of leads to the occurrence of numerous physical phenomena, among which the most important are:

1. Strong thermal gradients (10^7 - 10^{10} K/s) over the short distances resulting to melting and evaporating of very small quantity of material and the appearance of key-hole like cavity.
2. Movement of melted material due to viscous force, buoyancy force (density gradient) and Marangoni effect (surface tension gradient).
3. Mixing of molten materials (concentration gradient).

The aim of our work is to simulate temperature field, movement and mixing of molten materials and elements distribution in the welds. We use experimental data (work parameters, welding profile, and common element composition of the weld) to build the model. Then we compare the results of calculations with real copper distribution obtained by ESD analysis of the joint cross-section.

2. Description of the problem

We have compared the results for two joints (Table 1): 1) welding with low speed and low laser power (weak penetration) and 2) high speed and high laser power (full penetration).

We had used three step approaching scheme of modeling: model 1 that includes total geometry of cross-section and gives general picture of heating and movement in the welding pool (WP), model 2 that includes geometry of nail-head and describes heating,

movement and composition for each side between key-hole wall WP wall and model 3 that describes local diffusion of copper at the interfaces of WP.

Table 1: Operational parameters used in calculations

Parameter	Joint		
	1	2	
Power, W	P	800	2000
Welding speed, m/s	V	0,005	0,018
Beam radius, m	R	$1 \cdot 10^{-4}$	$1 \cdot 10^{-4}$
Focus	<i>f</i>	At the top surface	

2.1 Heat transfer

In model 1 we propose complex heat source that corresponds to key-hole mode of welding. First source is Gauss heat distribution applied to top-surface that depends of laser power and includes Beer-Lambert factor:

$$Q = \frac{P}{\pi \cdot R^2} \cdot a \cdot \alpha \cdot \exp\left(-\frac{x^2}{R^2}\right) \cdot \exp(-\alpha \cdot y)$$

And the second source is key-hole with the walls heated to temperature of vaporization of material [2]. The key-hole was considered as a cone with radius R that corresponds to laser beam radius.

The heat equation used includes the term of the latent heat of fusion:

$$\rho \cdot (c_p + D \cdot H_f) \cdot \vec{u} \cdot \vec{\nabla} T + \vec{\nabla} \cdot (-k \cdot \vec{\nabla} T) = Q$$

Term D is represented by Gauss distribution and normalized around the fusion temperature with half-width $\delta T = 50$ K:

$$D = \frac{\exp\left(-\frac{(T - T_F)^2}{(\delta T)^2}\right)}{\sqrt{\pi}(\delta T)^2}$$

The boundary condition for the walls of WP is T equal to fusion temperature of material.

For other surfaces the heat flux condition has been applied

$$\vec{\nabla} \cdot (-k \vec{\nabla} T) = h \cdot (T_{ambiant} - T)$$

where *h* is heat transfer coefficient (W/(K·m²)).

To consider the presence of two materials in WP we use additivity rule:

$$A = A_{Cu} \cdot C_{Cu} + A_{Fe} \cdot (1 - C_{Cu}),$$

where *C_{Cu}* is the common atomic fraction of copper and *A* is material parameter.

To avoid discontinuity in materials' properties (thermal conductivity, specific heat capacity and density) during phase transition the Heaviside functions have been used in model 1:

$$A = A_{solid} + (A_{liquid} - A_{solid}) \cdot \text{flc2hs}(T - T_f, \delta T)$$

Model 2 present top part of WP and has been made to calculate precisely velocity and element distribution. The molten material has a temperature $T_{\text{melting}} < T < T_{\text{vaporization}}$, so we consider condition of $T_{\text{vaporization}}$ for the wall of key-hole and T_{melting} for liquid/solid surface and heat flux for top surface. Inferior part of nail-head has thermal isolation condition. Model 2 presents only liquid state and material parameters has been takes as constants at additivity rule.

Model 3 presents dissolution of copper (melting at 1385 K) during the contact with molten steel (1720 K) at the copper side of the weld.

The materials' properties are assumed in Table 3.

2.2 Hydrodynamic equations

Modeling of the flow in the WP is based on the resolution of Navier-Stokes equations.

$$\rho \cdot (\vec{u} \cdot \vec{\nabla} T) \cdot \vec{u} = \nabla \cdot (-\rho + \eta \cdot (\vec{\nabla} u + (\vec{\nabla} u)^T)) + \vec{F}$$

$$\vec{\nabla} \cdot (\rho \cdot \vec{u}) = 0$$

The Boussinesq approximation is used to represent the buoyancy-driven flow:

$$F = \alpha \cdot g \cdot \rho \cdot (T - T_{\text{max}})$$

The boundary conditions for model 1 and 2 are follows: for walls of the key-hole and for metal/air interfaces $n \cdot u = 0$ (slip condition) and for walls of WP $u = 0$ (no-slip condition) have been applied. The condition of Marangoni convection has been applied to metal/air interfaces (using week formulation):

$$\eta \cdot \frac{du_x}{dy} = \gamma \cdot \frac{dT}{dx}$$

The properties of molten metal have been taken as constants. To consider the presence of two materials in WP we use additivity rule.

Model 3 does not include liquid flow.

2.3 Element distribution

Coupling of heat transfer, convection and diffusion processes permit to simulate elemental distribution in dissimilar welds. We do the simplification utilizing copper diffusion coefficient in liquid iron in Fick's law:

$$\nabla \cdot (-D \cdot \nabla c) = 0$$

We consider diffusion coefficient as a function of temperature:

$$D = D_0 \cdot \exp\left(-\frac{E}{R \cdot T}\right)$$

Table 2: Diffusion constants [3]

Constant		Cu in Fe
Diffusion coefficient, m ² /s	D	3 · 10 ⁻⁴
Activation energy, kJ/mol	E	225

At the model 2 the boundary condition for the wall of key-hole was given as medium copper concentration determined by element analysis. Concentration of copper for the walls of WP was

considered as 100% for copper and 0% for steel. For the others surfaces the condition of symmetry was applied.

At the model 3 we apply the same conditions but we neglect convection at WP interface.

3. Numerical approach

3.1 Mesh-based geometry

We use experimental data to create exact profile of weld cross-section (Figure 1). For model 1 we define two sections of meshing: fine meshing (20 μm) for the welding pool and coarse meshing (20 μm) for the rest. For model 2 (Figure 2, a) we examine only melting pool, so the meshing used is more fine – 5 μm. For model 3 we use also fine meshing (5 μm) for molted zone and coarser (20 μm) for the solid (Figure 2, b).

Table 3: Physical constants for the materials used in calculations (4)

Constant		Material	
		Cu	Steel
Fusion temperature, K	T _f	1356	1720
Evaporation temperature, K	T _v	2835	3013
Absorbance coefficient, %	a	1	30
Extinction coefficient, m ⁻¹	α	300	300
Latent heat of fusion, J/mol	H _f	13 · 10 ³	2,6 · 10 ⁵
Density (solid), kg/m ³	ρ _s	8700	7980
Density (liquid), kg/m ³	ρ _l	7940	7551
Heat capacity (solid), J/(kg · K)	Cp _s	385	433
Heat capacity (liquid), J/(kg · K)	Cp _l	350	734
Thermal conductivity (solid), W/(m · K)	k _s	400	8.116
Thermal conductivity (liquid), W/(m · K)	k _l	140	12.29
Thermal expansion coefficient, m/(m · K)	β	2,5 · 10 ⁻⁵	2,4 · 10 ⁻⁵
Surface tension temperature coefficient, N/(m · K)	γ	-1,7 · 10 ⁻⁴	-4,3 · 10 ⁻⁴
Dynamic viscosity, kg/(m · s)	η	0,0039	0,005

3.2 Numerical scheme

During continuous welding laser beam creates welding front that moves linearly and recreates the

similar transversal pattern of welding pool all long the specimen. We solve the models that represent such patterns (cross-sections) corresponding to maximum keyhole penetration. All the models had been solved with stationary solvers.

At the Model 1 velocity distribution in case of Marangoni effect has been calculated by stationary linear solver UMFPAK due to certain convergence problems in nonlinear solver. Models 2 and 3 have been solved by stationary nonlinear solver UMFPAK.

4. Results and discussions

The major specific feature of dissimilar weld it is asymmetry in shape and elementary composition that finally determines its mechanical resistance. High thermal conductivity and reflectivity of copper lead to formation of welds with only 10-20 % vol. Cu.

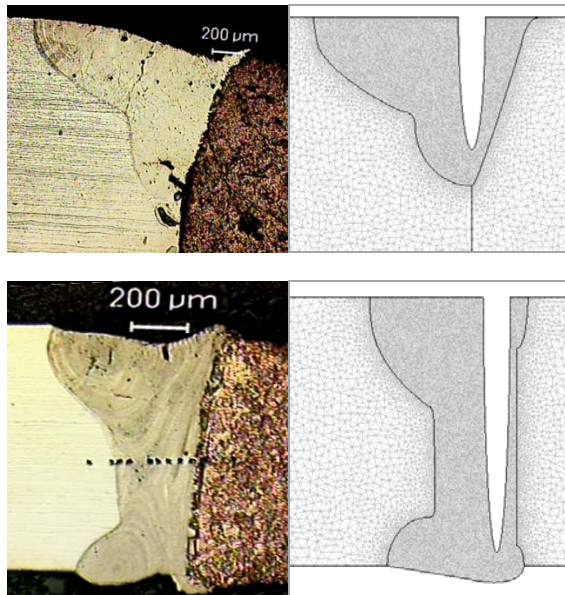


Figure 1: Mesh and geometry: model 1: joint 1 (top) and 2 (down).

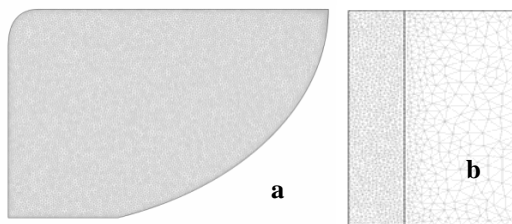


Figure 2: Mesh and geometry of models: a) model 2, b) model 3.

The joints 1 and 2 of model 1 (Figure 3) present heat gradient and give general look at velocity distribution. In both cases we see that at the top part of the weld convection is controlled by Marangoni effect (maximum velocity esteemed to be up to 10 m/s is in agreement with typical value [5]), that leads to horizontal propagation of WP to steel side (due to negative temperature coefficient of surface tension).

Big Marangoni number (Table 4) confirms crucial role of thermocapillary effect in formation of WP at the steel side. Value of Reynolds number indicates approaching to turbulent regime (10^5). In case of full penetration we observe second nail-head at the down part of steel side. At the thin part of WP only buoyancy convection is expected (the maximum calculated velocity is about 0,003 m/s).

Model 2 present precise velocity distribution in the nail-head of the welds. We calculate separately the parts of WP between key-hole and solid steel and between key-hole and solid copper. Maximum liquid steel velocity achieved between key-hole and solid steel at the air/metal interface is about 7 m/s for both cases (Figure 4), which corresponds to similar nail-head geometry. For joint 1 at the copper side we observe maximum velocity of steel/copper mixture about 5 m/s and thermocapillary convection localized at 200 μm top surface layer (Figure 5). For joint 2 copper side of WP is very thin and has not nail-head shape (due to high welding velocity), so we suspect that there is no Marangoni convection and buoyancy force creates very low speed flow ($3 \cdot 10^{-4}$ m/s).

Table 4: Dimensionless numbers calculated.

Numbers	Joint	
	1	2
Marangoni $Ma = \frac{L \cdot \gamma \cdot \Delta T \cdot \rho \cdot C_p}{\eta \cdot k}$	$1,2 \cdot 10^4$	$9,65 \cdot 10^3$
Reynolds $Re = \frac{L \cdot V \cdot \rho}{\eta}$	$1,80 \cdot 10^4$	$1,45 \cdot 10^4$

L – WP length, m, V – welding speed, m/s.

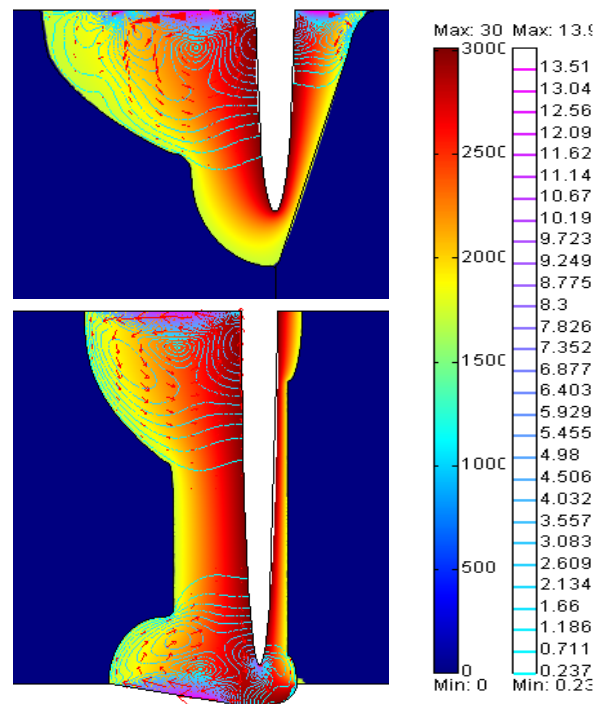


Figure 3: Thermal distribution and velocity field for model 1: joint 1 (top) and 2 (down).

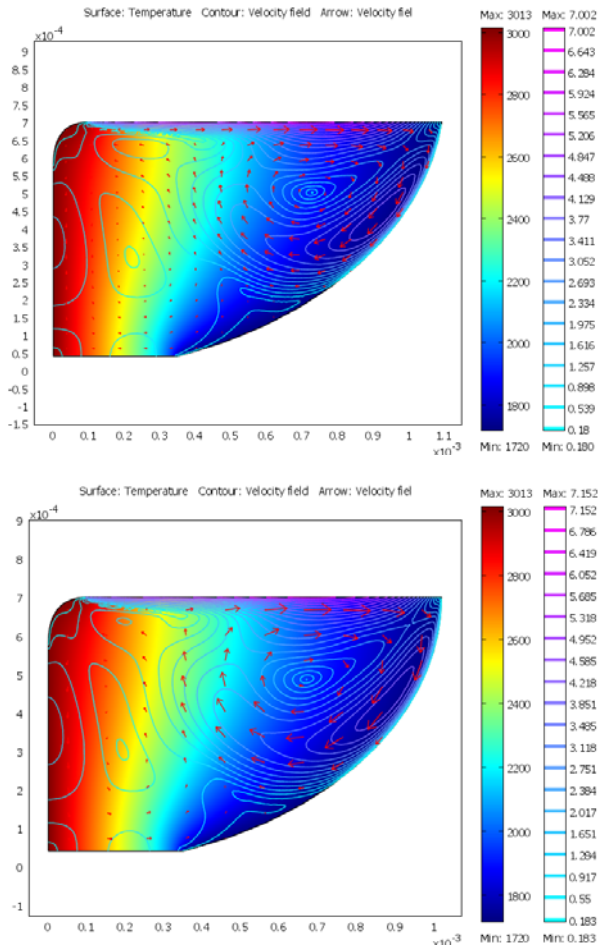


Figure 4: Thermal distribution and velocity field for model 2, steel side, top nail-head: joint 1 (top), joint 2 (down).

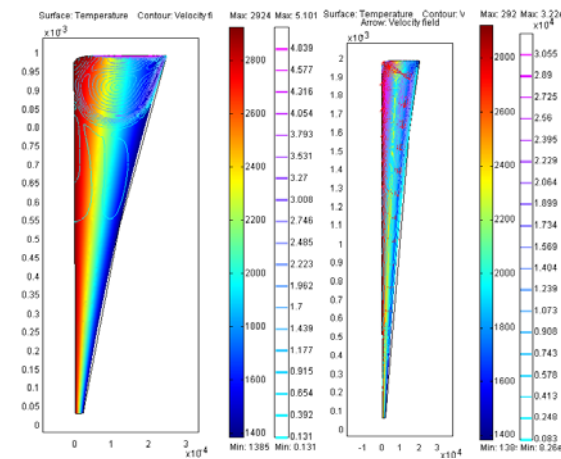


Figure 5: Thermal distribution and velocity field for model 2, copper side: joint 1 (left), joint 2 (right).

The distribution of copper due to ESD-analysis at the transversal cut of weld has been compared with results of simulation (model 2). For joint 1 due to low speed of welding full homogenization of WP is achieved (common copper concentration is 10 at. %, partial penetration). For joint 2 due to high laser power melting of copper is more effective (17,5 at. %, full penetration) and high speed of welding leads to appearance of certain unhomogeneity at the WP.

The calculated concentrations of Cu appeared to be very similar to reality (Figure 6).

We suppose that propagation of Cu at the copper side of WP happens mainly by diffusion in molten steel and convection mixing can be neglected. Model 3 describes diffusion process at copper / WP interface without influence of liquid convection. Good correspondence between calculated distribution and results of analysis confirm our hypotheses (Figure 7).

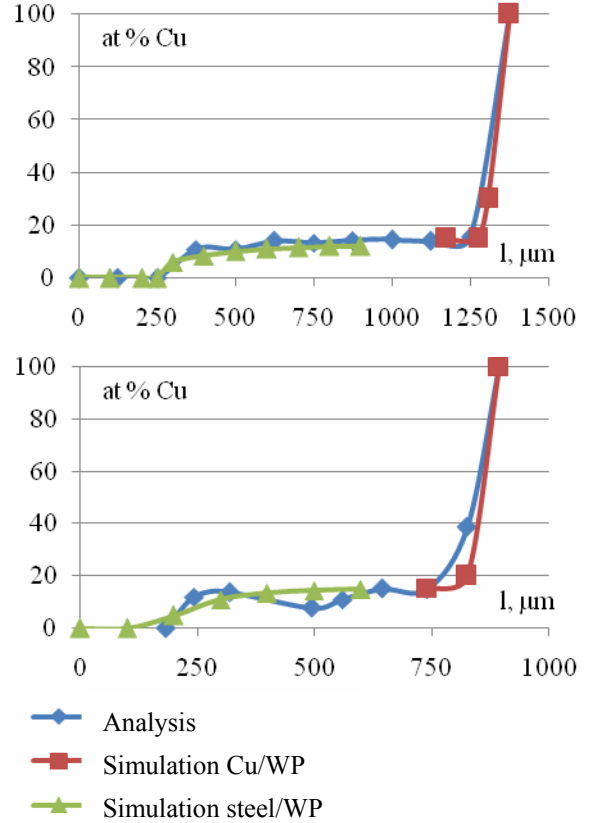


Figure 6: Copper distribution in the welds obtained by ESD analysis and simulated using model 2: joint 1 (top), joint 2 (down).

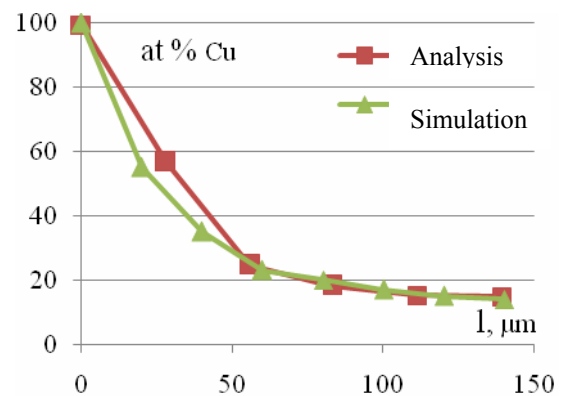


Figure 7: Diffusion of copper in molten steel for copper side of WP, joint 2.

5. Conclusions and prospects

The numerical models of heat and matter distribution at copper/steel welds permitting to better understand dissimilar welding process. The models

proposed do not demand long time of calculations but present simplifications and leave out of account forces parallel to welding direction.

Passage to time dependent mode and moving mesh geometry is necessary to realize more flexible and realistic models.

6. References

1. H. Akamatsu, M. Yatsuzuka, Simulation of surface temperature of metals irradiated by intense pulsed electron, ion and laser beams, *Surface and Coatings Technology*, 169 –170, 219–222 (2003)
2. E. Dumord, J.M.Jouvard, D. Grevey, Modeling of deep penetration welding : Application to the cw Nd:YAG laser welding of X5Cr.Ni.18-10, *Laser in Engineering*, Vol 9., pp. 1-21 (1999)
3. C.J.Smithels, *Metal Reference book, 4th ed.*, Metal Powder Industry Federation, Princeton, NJ (1994)
- 4 www.matweb.com
- 5.J.M. Drezet, S. Pellerin, C. Bezencon, S. Mokadem, Modelling the Marangoni convection in laser hest treatment, *Journal de Physique IV*, 4, 1-8 (2004)